BIOCOMPATIBILITY IMPROVEMENT OF UNS S32750 DUPLEX STAINLESS STEEL BY INDUCTIVELY COUPLED RADIOFREQUENCY PLASMA NITRIDING

André Augusto Bonfante de Souza[0000-0001-5605-5033], UTFPR, eng.and.s@gmail.com
Thiago Dunaiski de Souza [0000-0002-9497-4054], UTFPR, thiagodunaiski@gmail.com
Euclides Alexandre Bernardelli [0000-0003-1991-3056], UTFPR, ebernardelli@utfpr.edu.br
Márcio Mafra[0000-0002-5866-6863], UTFPR, mafra@professores.utfpr.edu.br

Abstract. *Nitriding is a thermochemical treatment based on nitrogen diffusion on ferrous alloys to improve its mechanical performance and its corrosion behavior. The increase in nitrogen content during nitriding promotes surface phase transformation of stainless steels, leading to increased biocompatibility of the material. The present work evaluated the effect of temperature on the inductively coupled radio frequency plasma nitriding of UNS S32750 duplex stainless steel. The samples were treated in inductively coupled radio frequency plasma with direct current bias (RF-DC) on a tubular reactor. Plasma nitriding treatments were carried out for 4 hours at 400 and 450 ºC (673 and 723 K), resulting in expanded austenite layer thickness up to 10,5 µm and average microhardness up to 1767 $HK_{0,05}$. The maximum nitrogen content obtained was approximately 11,5%wt. It was observed that nitrogen diffusion is phase-dependent, but, at higher temperatures, expanded-phase layer formed on both previous phases have equivalent nitrogen content.*

Keywords*: duplex stainless steel, radiofrequency plasma, inductively coupled plasma, stainless steel biocompatibility, plasma nitriding.*

1. INTRODUCTION

Duplex stainless steels grades are referred to have two different phases in their microstructure, with a minimum chromium content of 18%wt. The proportions of each solid phase vary accordingly, amongst other factors, on the chemical composition of each alloy, accordingly to Gunn (1997). During nitriding, it is expected a superficial expanded metastable phase with high nitrogen content, which promotes increasing in hardness, wear and fatigue resistance as pointed by Borgioli *et al.* (2006). In general, it is reported that higher nitriding temperatures (above 400 ºC) lead to precipitation of chromium nitrides, local depletion of chromium, decreasing corrosion resistance, in a phenomenon called sensitization, as described by authors such as Kurelo *et al.* (2015) and Oliveira *et al.* (2018).

Recent works, such as the study of austenitic stainless steels by Gil *et al.* (2006) and Yun-Ho *et al.* (2012) have shown that biocompatibility is directly associated with material surface. As pointed by Gil *et al.* (2006), a rough surface with N-H radicals improves wettability, protein adsorption and, thus, blood-compatibility. In the case of duplex stainless steels, surface expanded austenite phase formation is important for the biocompatibility of the material. Furthermore, duplex stainless steels are harder than one-phase stainless steels in general. Hence, the duplex grade becomes interesting for biomechanical applications, reducing the total mass required for a specific use.

In this context, the present work intends to contribute to the understanding of the biocompatibility improvement caused by the radiofrequency inductively coupled plasma nitriding of a duplex stainless steel.

2. EXPERIMENTAL

UNS S32750 super duplex stainless steel (SDSS) samples (20x22x2mm) 347±11 $HK_{0,050}$ were grounded up to #1200 mesh and polished with 1,0 µm Al_2O_3 suspension. Subsequently, samples were properly cleaned and introduced into a tubular reactor (960mm length, 36mm diameter). Inductively coupled radiofrequency plasma (RF-ICP) was generated by an external coil (8 turns) coupled to a radiofrequency power supply (250 W). An external DC power supply biased the samples, which was used in the sputtering step and, for some samples, polarization during nitriding.

A previous sputtering phase was carried out by DC plasma at 300 ºC, – 620 V for 40 minutes in a 20% Ar 80% H_2 atmosphere. Plasma nitriding occurred at 400 ºC and 450 ºC for 4 hours in a 70% N_2, 20% H_2 and 10% Ar atmosphere, with a total flux of 50 sccm. The pressure varied between treatment conditions from 0,38 torr (51 Pa) for samples LF (400 ºC, floating potential), L200 (400 ºC, - 200 V bias) and HF (450 ºC, floating potential) to 0,50 torr (66 Pa) for sample H200 (450 ºC, - 200 V bias).

For the biased configuration, a – 200 V DC voltage was applied between the sample holder and a counter-electrode throughout all the nitriding phase of the treatment. All experimental conditions for nitriding phase have been summarized in Tab. (1). The higher pressure observed during treatment of sample H200 was due to experimental variations.

Table 1. Nitriding phase parameters for each sample.

Parameter	Sample			
	LF	L200	HF	H200
Temperature ºC	400	400	450	450
Pressure (Pa)	51	51	51	66
Atmosphere Composition (% vol.)	70% N_2 - 20% H_2 -10% Ar			
RF Power (W)	250			
DC bias potential (V)	Floating potential	-200	Floating potential	-200
Nitriding time (h)	4			

After nitriding, the samples were cooled and analyzed regarding its microhardness (Knoop), developed phases and compounds (X-Ray Diffraction – XRD) and nitrogen content (Wavelenght Dispersive Spectroscopy – WDS).

Microhardness measurements were made utilizing a Shimadzu HMV-2 with 50g load and Knoop indenter. The average values obtained for each phase were measured on the surface of the samples, thus, not representing profiles.

For XRD a Shimadzu XRD-7000 was utilized employing the following parameters: Cu kα radiation (λ = 1.5418Å), 2theta ranging between 35-75 degrees and scan rate of 1 degree per minute. A low-angle configuration (5 degrees) was used for the incident beam in relation to the sample surface. For WDS analysis, an Oxford Instruments IncaWave 500 coupled to a Zeiss Evo MA15 SEM with 5 kV voltage was used. Nitrogen content measurements from WDS are also relative to the surface, hence, the single average value for each sample (Fig. (5)). SEM images were also obtained through Zeiss Evo MA15 with a BSD detector.

3. RESULTS AND DISCUSSION

The samples nitrided without DC bias (LF and HF) did not show a visible nitrided layer. As shown in Fig. (1), XRD diffractograms did not reveal observable expanded austenite (γ_N peak asymmetry and/or shift) on samples LF and HF.

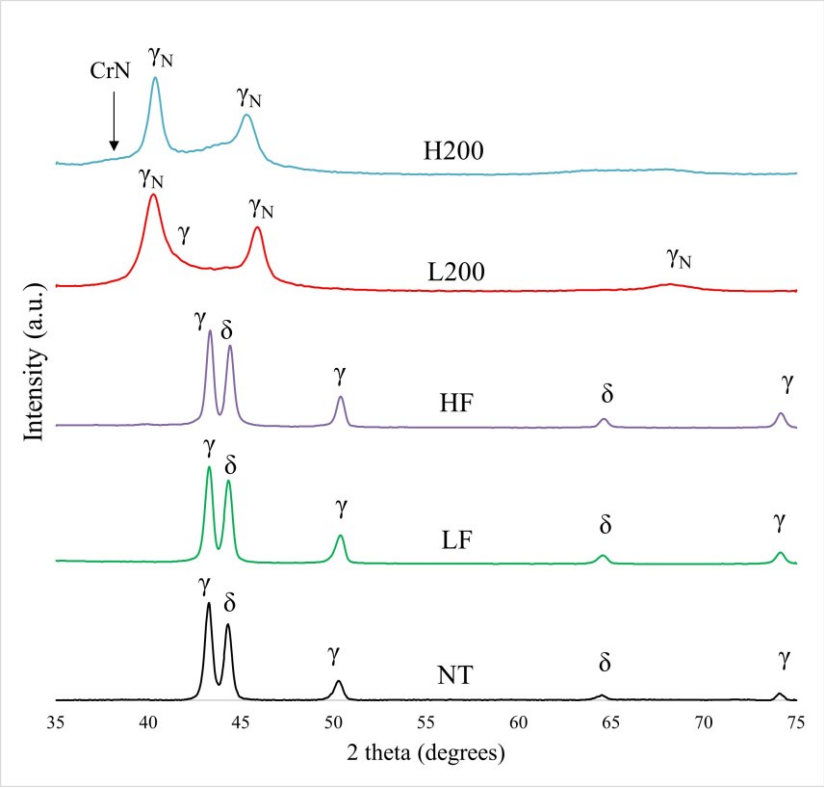

Figure 1. X-ray diffractograms of samples treated under floating potential (LF and HF) and -200 V DC bias at 400 and 450 ºC. Non-treated material (black line) as reference.

However, expanded austenite peak shifts of L200 and H200 (DC biased samples) were significant. It is also observed in Fig. (1) the absence of ferritic peaks (near 45 and 65 degrees) for L200 and H200 samples. This absence can be related to the transformation of ferrite to expanded austenite, as observed by Oliveira et al. (2018) at the same temperature.

Also, there is a possibility that the disappearance of δ peaks is related to the expansion of ferritic lattice of superficial δ-grains due to nitrogen supersaturation, as pointed by Pinedo, Varela and Tschiptschin (2013) or iron nitride precipitation, as observed by Tschiptschin et al. (2017). Lattice expansion of δ-Fe would cause peak flattening and enlargement, as it can be observed in Fig. (1) for samples L200 and H200. No chromium nitride precipitation was observed at 400 ºC, being observed only on sample H200 (-200 V bias, nitrided at 450 ºC).

Figure (2) shows SEM cross-section images of sample H200. Sample H200 average layer thickness was 10,5±1,3 and 10,0±0,5 µm for δ-Fe and γ-Fe, respectively. The biased sample treated at 450°C has shown a more uniform layer thickness (Fig. (2-a)) then biased sample treated at 400°C (Fig. (3)). It is worth noticing that the referred phases ferrite (δ-Fe) and austenite (γ-Fe) does not necessarily correspond to the present phases on the layer since, according to Fig. (1), phase transformation occurred.

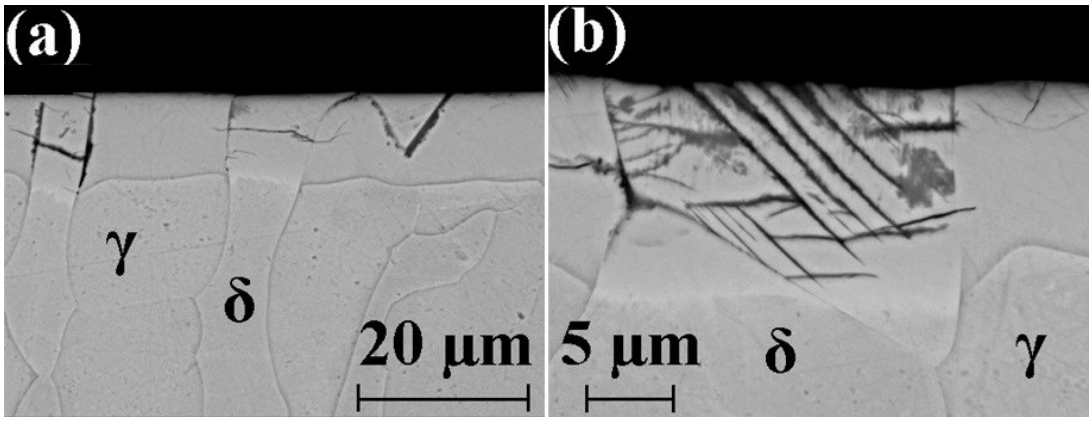

Figure 2. SEM of sample H200 (cross-section). In (a), dark regions can be attributed to the high residual stress induced by nitrogen diffusion and phase transformation and/or chromium nitride precipitation. In (b), parallel lines indicate nitrogen diffusion at preferential crystallographic orientation. Magnification 4000x (a), 8000x (b).

Parallel lines can be observed on the layer formed at δ-grain (Fig. (2-b)). These lines can be related to the diffusion of nitrogen at preferential crystallographic orientation, as pointed by Sphair (2017). Dark regions across these lines can also be associated with chromium precipitation, as observed by Tahchieva, Llorca-Isern and Cabrera (2019) on plasma nitriding of duplex grade of stainless steels.

Figure (3) shows SEM of DC biased nitriding treatment at 400 ºC (sample L200). As previously mentioned, the formed layer on sample L200 was not as uniform is terms of thickness as the formed layer on sample H200. This can be explained by the lower diffusion when compared to the higher temperature of 450 ºC and slower kinetics of phase transformation.

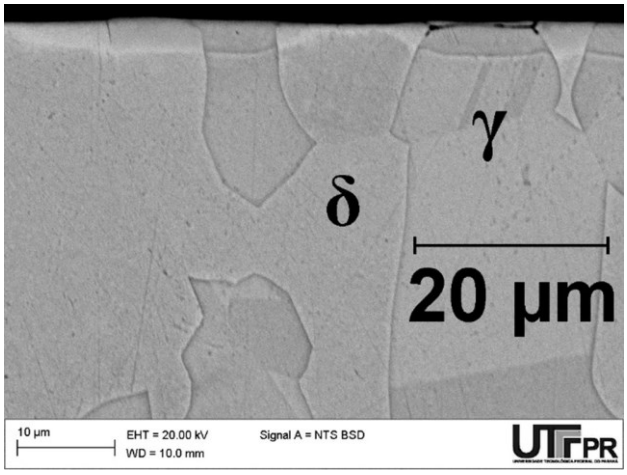

Figure 3. Cross-section SEM denoting layer thickness variations between phases for sample L200. Magnification 4000x.

Nitrided layer thickness of sample L200 were 3,0±1,2 and 3,6±0,5 µm for δ-Fe and γ-Fe, respectively. It is also noticed that, in regions close to the grain interface, the layer is thicker in δ-grains and thinner on γ-grains. This result suggests that intergranular diffusion of nitrogen from the nitride layer from γ-grains to δ-grains occurs during the treatment. This phenomenon is corroborated by Zimmermann (2014). For sample H200, seen in Fig. (2), layer thickness differences between phases, including the interface region between grains, is less expressive. According to Alphonsa, Mukherjee and Raja (2018), this can be attributed to the faster kinetics of ferrite phase transformation.

Figure (4) presents the average microhardness over each phase of the bulk material for each treatment condition. Non-treated microhardness of the material was also plotted and corresponds to the blue dashed line (NT). L200 sample presented expanded austenite layer with hardness increase from 347±11 $HK_{0,050}$ (non-treated) to 990±185 on ferritic and 765±64 on austenitic phases and sample H200 1767±234 on ferritic and 1009±277 on austenitic phase.

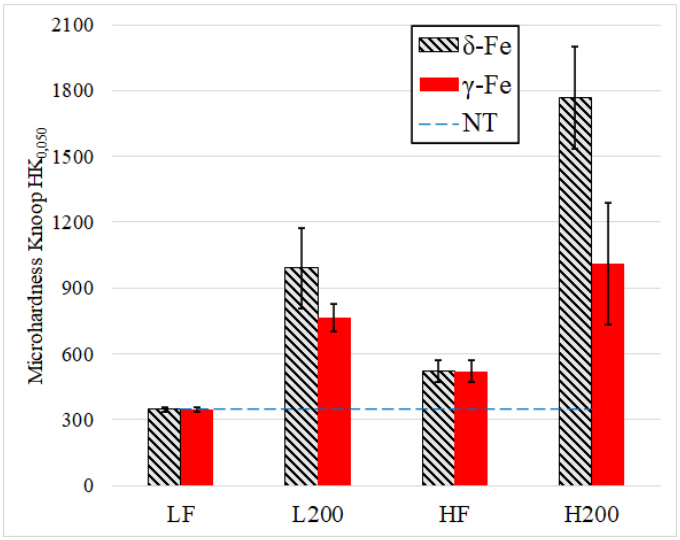

Figure 4. Knoop microhardness for samples LF, HF, L200 and H200 as function of bulk grain phases. Blue NT line corresponds to the non-treated material.

Average nitrogen content (% weight) was detected by WDS for each treatment and are summarized in Fig. (5). For samples treated under floating potential, the average nitrogen content was 1,2 ±0,0% (δ-Fe), 0,9±0,2% (γ-Fe) for sample LF and 2,01±0,2% (δ-Fe), 1,45±0,3 (γ-Fe) for sample HF. The highest nitrogen content was obtained for sample H200, 11,0±1,4% (δ-Fe), 11,2±1,0% (γ-Fe). Sample L200 average nitrogen content was 7,38±0,4% (δ-Fe), 11,5±0,2% (γ-Fe). The nitrogen introduced on the surface of sample HF was able to increase material hardness, even though it did not produce an observable expanded layer.

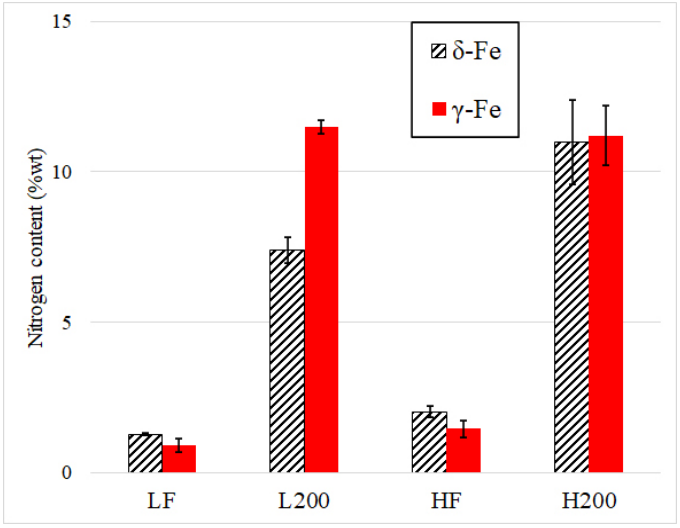

Figure 5. Nitrogen content of samples nitrided LF, HF, L200 and H200 as function of grain phases of the bulk material.

Higher nitriding temperature of 450 ºC promoted higher overall nitrogen content of the layer. In addition, nitride layer on γ-grains presented roughly the same amount of nitrogen (at least on the top of the layer) on both temperatures for biased treatments, indicating nitrogen saturation due to the higher nitrogen solubility on γ compared to δ phase.

Comparing the nitrogen content of the layer formed over each grain phase of the bulk material with the microhardness of the layer, one can be seen, at 450 ºC, that the layer formed over δ phase presented substantial hardness increase comparing to the layer formed over γ phase, despite the similar nitrogen content.

A plausible explanation for that resides on the additional residual stress induced by nitrogen content and phase transformation in δ. Another possible explanation is related to the expanded ferrite described in the works by Pinedo *et al.*, (2013) and Borgioli *et al.*, (2016). Lastly, it is possible that iron nitrides were formed preferably over δ phase, as pointed out by Oliveira *et al.*, (2018). Although the XRD did not show iron nitride peaks, they are difficult to detect and may have formed preferentially over the ferritic phase of the material.

It is important to point out that the sample L200 presented similar nitrogen content to H200, indicating that austenite phase had better nitrogen diffusion compared to ferrite phase of the material.

The harder layer obtained on sample H200 is related to the thicker layer for this sample in comparison to L200, due to the promotion of better mechanical support for microhardness measurements. For biased samples, it is also noticeable that the microhardness of the layer formed over δ-grains is significantly harder than over γ-grains. Harder layer formed on ferrite grains can be attributed, accordingly to Borgioli *et al.*, (2016), to plastic deformation caused by phase transformation to expanded austenite. It is observed that the bigger the layer thickness, the bigger the difference observed between δ-grains and γ-grains microhardness.

In summary, it is noticed that the increase in temperature promotes a higher nitrogen content diffused on the material surface and that the DC bias increases nitriding species concentration on the surface during the treatment.

Another important aspect to the biocompatibility of the material resides in its roughness. Figure (6) shows a comparison of all samples nitrided. It is evident that the DC bias was the major parameter for surface topography alteration.

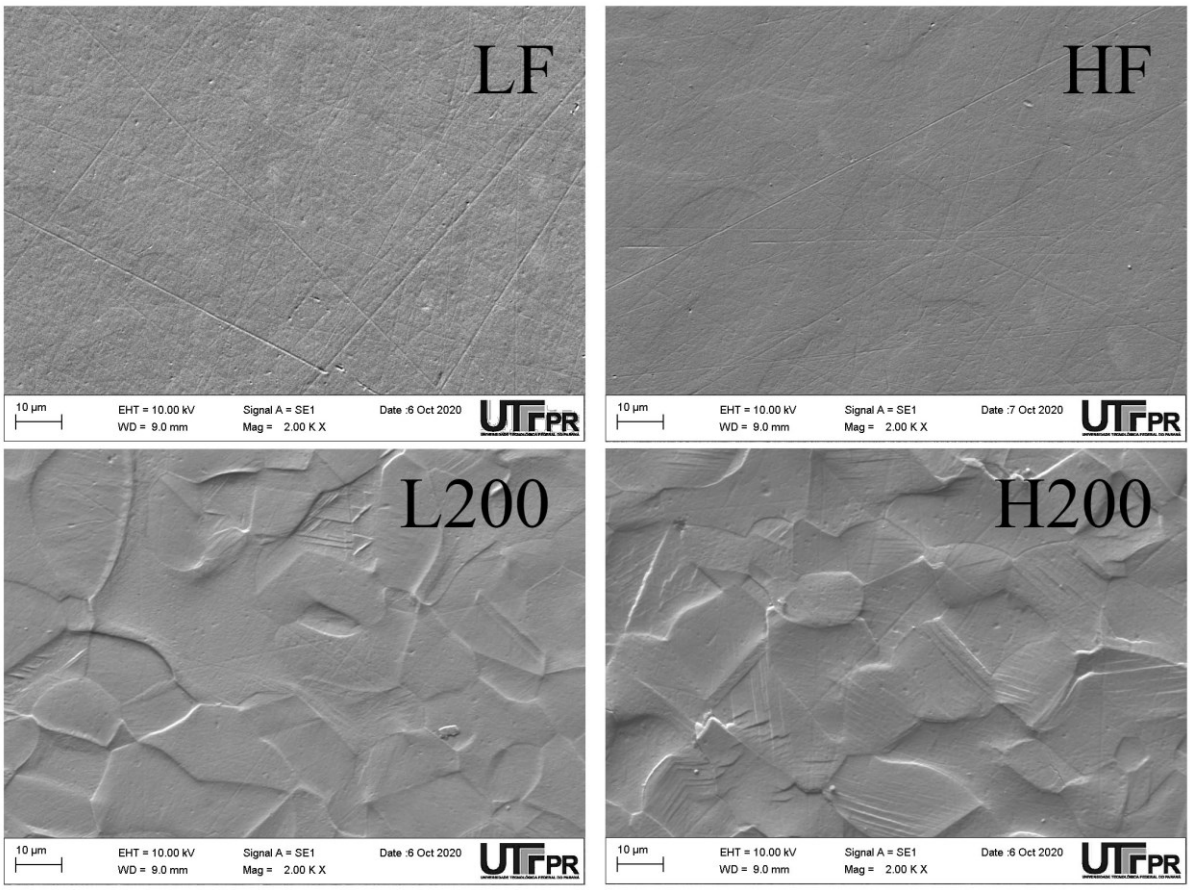

Figure 6. Surface topography of samples LF, HF, L200 and H200.

For the austenitic phase, at 450 ºC it is observed that the temperature increase does not promote increase in nitrogen content. However, for the ferritic phase, the increase is significant. This is due to the rapid saturation of the material's

austenitic phase, which consequently promotes intergranular nitrogen diffusion to the ferritic phase. At 400 ºC, this phenomenon contributes less to the diffusion process. At the higher temperature (450 ºC), intergranular diffusion occurred in a greater rate. Thus, phase transformation from ferritic into expanded austenite promoted greater nitrogen content, layer thickness and uniformity, leading to a harder surface. Microhardness measurement of the surface on different grain phases (previous phases of the material) was important to point out that even the higher nitrogen content on the expanded austenite from an austenite grain in comparison to the ferrite grain does not increase its hardness so expressively as it does on the expanded austenite from ferrite grain region.

The control of nitrogen content on the treated surfaces can be used to create surfaces useful to biomechanical applications. As pointed by Basso et al. (2009), expanded austenite magnetic transition occurs at a threshold of approximately 14±2%wt. nitrogen, shifting its biocompatibility. Since the process did not promote any sample to this level of nitrogen content, the magnetic shift of the surface did not change, even though it was not assessed.

The pressure increase (from 51 to 66 Pa) may have contributed to the nitrogen content increase on sample H200 (in comparison to L200) due to the higher concentration of nitriding species. Still, the major factors were, undoubtedly, the temperature increase and DC bias. The present work demonstrates the feasibility to treat SDSS in inductively coupled plasmas to obtain a bio-compatible surface. DC bias of the samples has been shown to be helpful to ICP low temperature nitriding.

4. REFERENCES

Alphonsa, J.; Mukherjee, S.; Raja, V. S., Study of plasma nitriding and nitrocarburizing of AISI 430F stainless steel for high hardness and corrosion resistance. **Corrosion Engineering Science and Technology,** 2018. v. 53, p. 51–58.

Basso, R. L. O.; Pimentel, V. L.; Weber, S.; Marcos, G.; Czerwiec, T.; Baumvol, I. J. R.; Figueroa, C. A. Magnetic and structural properties of ion nitrided stainless steel. **Journal of Applied Physics**, 2009. v. 105, p. 124914 1-5.

Borgioli, F.; Galvanetto, E.; Bacci, T. Low temperature nitriding of AISI 300 and 200 series austenitic stainless steels. **Vacuum**, 2016. v. 127, p. 51–60.

Borgioli, F.; Galvanetto, E.; Bacci, T.; Pradelli, G. Glow discharge nitriding of AISI 316L austenitic stainless steel: Influence of treatment pressure. **Surface and Coatings Technology**, 2006. v. 200, p. 5505-5513.

Gil, L.; Jiménez, L.; Leon, O.; Guevara, R.; Staia, M. H. Corrosion performance of the plasma nitrided 316L stainless steel. **Surface and Coatings Technology**, 2006. v. 201, p. 4424-4429.

Yun-Ho, L.; Wen-Chien, L.; Keng-Liang, O.; Cheng-Ming, L.; Pei-Wen, P. Hemocompatibility evaluation of plasma-nitrided austenitic stainless steels at low temperature**. Surface and Coatings Technology**, 2012. v. 206, p. 4785–4790.

Gunn, R.N., 1997. **Duplex Stainless Steel**, Abington: Abington Publishing. Cap 1, p.1-11.

Kurelo, B. C. E. S.; De Souza, G. B.; Da Silva, S. L. R.; Serbena, F. C.; Foerster, C. E.; Alves, C. Plasma nitriding of HP13Cr supermartensitic stainless steel. **Applied Surface Science**, 2015. v. 349, p. 403–414.

Oliveira, W. R.; Kurelo, B. C. E. S.; Ditzel, D. G.; Serbena, F. C.; Foerster, C. E.; De Souza, G. B. On the S-phase formation and the balanced plasma nitriding of austenitic-ferritic super duplex stainless steel. **Applied Surface Science**, 2018. v. 434, p. 1161– 1174.

Pinedo, C. E.; Varela, L. B.; Tschiptschin, A. P. Low-temperature plasma nitriding of AISI F51 duplex stainless steel. **Surface and Coatings Technology**, 2013. v. 232, p. 839–843.

Sphair, A. C. **Austenitic Stainless Steel Plasma Nitriding with pulsed nitrogen flow (in Portuguese)**. 2017. Master's Dissertation (Graduate Program in Mechanical and Materials Engineering) - Federal Technological University of Paraná, Brazil.

Tahchieva, A. B.; Llorca-Isern, N.; Cabrera, J. M. Duplex and superduplex stainless steels: Microstructure and property evolution by surface modification processes. **Metals**, 2019. v. 9, n. 3.

Tschiptschin, A. P.; Nishikawa, A. S.; Varela, L. B.; Pinedo, C. E. Thermal stability of expanded austenite formed on a DC plasma nitrided 316L austenitic stainless steel. **Thin Solid Films**, 2017. v. 644, n. June, p. 156–165.

Zimmerman, M. R. B. **Plasma nitriding of 2205 duplex steel (in Portuguese).** 2014. Master's dissertation (Graduate Program in Mettalurgic and Materials Engineering) - Polytechnic School of the University of São Paulo, Brazil.

5. ACKNOWLEDGMENTS

Authors are grateful to NESAP for the SDSS samples, CMCM-UTFPR and PUC-PR for characterizations, to CAPES under process 88882.431970/2019-01 and CNPQ under process 430088/2016-7 for the financial support.

6. RESPONSIBILITY NOTICE

The authors are solely responsible for the printed material included in this paper.